Int. J. Heat Mass Transfer. Vol. 31, No. 7, pp. 1345–1355, 1988
Printed in Great Britain

0017–9310/88 $3.00 + 0.00

Experiments on isothermal and non-isothermal evaporation from partially filled, open-topped vertical tubes

E. M. SPARROW and G. A. NUNEZ
Department of Mechanical Engineering, University of Minnesota, Minneapolis, MN 55455, U.S.A.

(*Received* 23 *September* 1987 *and in final form* 5 *January* 1988)

Abstract—Experiments were performed to provide a critical test of analytical/numerical models for predicting evaporation from an open-topped vertical tube partially filled with a liquid. Separate apparatuses were used to achieve evaporation under either isothermal or non-isothermal conditions. The experiments were performed for water evaporating into air which contained water vapor. The experimental work was supplemented by the numerical implementation of the models using the ambient conditions of the experiments as input. Excellent agreement was found to prevail between the experimentally determined and numerically predicted Sherwood numbers. This finding, along with other comparisons, validated the models. For isothermal evaporation, the validation established that account must be taken of natural convection in the gas–vapor space above the liquid surface and that pure diffusion is an insufficient description of the transport process. For non-isothermal evaporation, it was established that in addition to natural convection in the gas–vapor space, it is necessary to account for thermal radiation at the bounding surfaces of the space and for natural convection in the liquid pool.

INTRODUCTION

THIS PAPER describes an experimental investigation of evaporation from a liquid pool, which partially fills a circular tube, into an otherwise quiescent ambient. The experiments were performed with water as the evaporating liquid and with water-vapor-containing air as the ambient. The tube was vertical and its upper end was open to the ambient. Basically, the evaporation was driven by the difference in the water vapor concentrations at the surface of the water pool and in the ambient, although different transfer mechanisms participated depending on the operating conditions.

Two generic classes of operating conditions were considered. In one, the system was virtually isothermal, so that the participating transport processes were mass diffusion and buoyancy-driven fluid flow (i.e. natural convection) in the air–vapor mixture in the space between the liquid surface and the top of the tube. The buoyancy was created by concentration differences.

The second generic case was non-isothermal evaporation. Here, the temperature of the liquid surface was depressed below the ambient temperature. While mass diffusion continued to operate as before, the natural convection in the air–vapor space was now driven by buoyancy which resulted from both concentration and temperature differences. Furthermore, the non-isothermal operating conditions activated radiant interchange among the bounding surfaces of the air–vapor space and with the ambient. Natural convection in the water pool was also activated, as was conduction in the tube wall, in the insulation surrounding the tube, and in the insulation container.

The isothermal and non-isothermal operating conditions were achieved by the use of different apparatuses, as will be described later.

The experimental work to be reported here represents the second and final phase of a two-part study of the problem of evaporation from a partially filled tube to a quiescent ambient. The first part of the study, reported in ref. [1], was an in-depth modeling and computational effort which examined the following issues:

(1) isothermal vs non-isothermal evaporation;
(2) interactions between the velocity, mass fraction, and temperature fields in the gas–vapor space in the tube and in the ambient;
(3) natural convection in the gas–vapor space;
(4) radiative interchange in the gas–vapor space;
(5) natural convection in the liquid pool;
(6) conduction in the insulation surrounding the tube, in the tube wall, and in the insulation container.

These various effects were explored numerically in ref. [1] by means of a number of typical cases which were characterized by realistic operating conditions but which were not specific to any of the experimental runs.

Here, the appropriate models will be numerically implemented for the specific operating conditions of the experiments. As a consequence, the presentation of results will include both experimental data and numerical predictions, which will be compared whenever possible. The results to be presented are:

NOMENCLATURE

A	surface area, $\pi d^2/4$
D	mass diffusion coefficient
d	inside diameter of tube
g	acceleration of gravity
K	mass transfer coefficient, equation (6)
L	distance between liquid surface and top of tube
M	mass of water in tube
ΔM	evaporated mass
p	pressure
R	inner radius of tube
Ra	Rayleigh number, equation (8)
r	radial coordinate
Sc	Schmidt number
Sh	Sherwood number, Kd/D
T	temperature
T_s	temperature at liquid surface
T_∞	ambient temperature
u	axial velocity component
x	axial coordinate.

Greek symbols

μ	viscosity
ν	kinematic viscosity
ρ	density
ρ_s	mixture density adjacent to liquid surface
$\rho_{wv,s}$	density of water vapor adjacent to liquid surface
$\rho_{wv,\infty}$	density of water vapor in ambient
ρ_∞	ambient mixture density
τ	duration of evaporation run
ϕ_∞	ambient relative humidity.

Subscripts

a	dry air
db	dry bulb
s	liquid surface
sat	saturation state
wv	water vapor
∞	ambient.

(1) evaporation rates, expressed in dimensionless form via the Sherwood number;

(2) the temperature at the surface of the water pool;

(3) patterns of fluid flow in the air–vapor space in the tube and in the ambient;

(4) velocity profiles in the air–vapor space in the tube.

A more extensive presentation of results is available in the thesis [2] on which this paper is based. The literature survey reported in ref. [1] applies equally well here and need not be repeated.

EXPERIMENTAL APPARATUS AND PROCEDURE

Laboratory characteristics

A necessary prerequisite for the successful execution of the experiments was that they be performed in a laboratory in which the air was quiescent, the temperature and water vapor content (i.e. the humidity) were constant over a long period of time, and where both artificial lighting and daylight could be fully suppressed. These requirements were completely fulfilled.

The laboratory was, in fact, a room within a room. It was situated in a basement, away from exterior walls, and windowless. Neither heating nor cooling ducts passed into the room nor were there grilles or openings for ventilation. Its walls, ceiling, and floor were insulated with a 46-cm-thick layer of cork. The total volume of the room was about 70 m^3, and it contained various objects having a large aggregate heat capacity.

The unique combination of insulation, isolation, and large heat capacity made for unusual thermal stability. Furthermore, the moisture absorbing capability of the cork walls acted to stabilize the humidity.

Evaporation apparatus

As was noted in the Introduction, two different apparatuses were used to achieve the desired isothermal and non-isothermal modes of operation. Distilled water served as the evaporating liquid in all the experiments.

The isothermal experiments were performed in a specially fabricated aluminum tube which was used without insulation. Aluminum was selected because of its high thermal conductivity. The combination of an aluminum tube and the absence of insulation was intended to minimize the thermal resistance between the evaporating liquid and the ambient, thereby enabling the heat necessary for the evaporation process to be supplied at virtually zero temperature difference.

The tube had an i.d. of 3.80 cm, a wall thickness of 0.32 cm, and a variable length. The variable length feature was achieved by synthesizing the tube from either one, two, or three sections. Figures 1(a) and (b) illustrate the one- and three-section configurations of the tube. One of the sections was a cup-like container, and the others were sleeve-like extensions which were fitted atop of it. As indicated in Fig. 1, the water pool was always confined to the cup-like portion of the tube, regardless of whether one, two, or three sections were used.

The foregoing observation leads into the rationale for the composite nature of the tube. It was desired

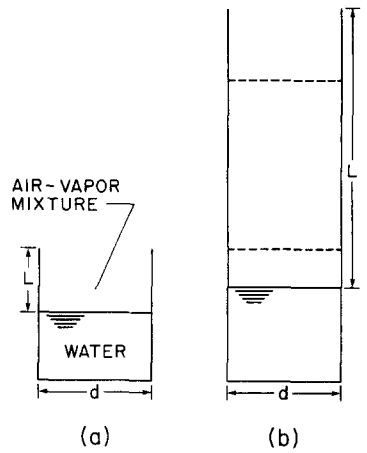

FIG. 1. Configurations of the tube for the isothermal evaporation experiments: (a) one-section configuration; (b) three-section configuration.

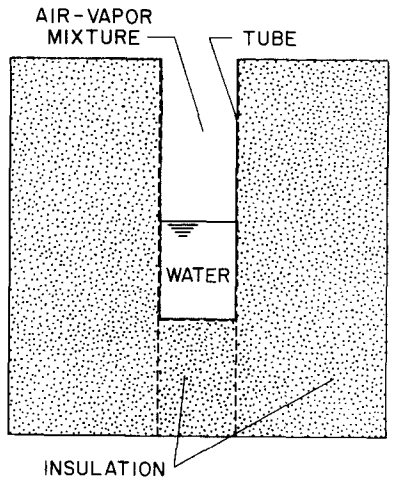

FIG. 2. Apparatus setup for the non-isothermal evaporation experiments.

to make use of a highly accurate analytical balance with a capacity of 200 g for measuring the mass of the tube and its contents before and after an evaporation run. Had the tube been one piece, its mass plus that of the water would have exceeded the capacity of the balance. This suggested a composite tube with a properly sized lower portion to match the weighing capacity of the balance.

As indicated in Fig. 1, the distance between the surface of the water and the top of the tube is denoted by L and the i.d. by d. With the tube empty, the largest L/d of the composite tube was equal to about 3.3.

To prevent electrolytic action between the water and the aluminum, the inner surfaces of the cup-like portion of the tube were lightly spray-painted and then polished to a high degree of smoothness with 1200-grit lapping compound. Continuity of the tube surface at the junctions of the various sections was ensured by hand-fitting operations—sanding and subsequent polishing.

For the non-isothermal evaporation experiments, the apparatus was designed to maximize the depression of the temperature of the water surface relative to the ambient temperature. To this end, the setup illustrated in Fig. 2 was used. The containment tube was made of polyethylene (rather than from a metal), and the tube was surrounded by a large volume of powder-type insulation (silica aerogel) having a nominal thermal conductivity about 20% less than that of air. The use of a non-metallic tube and low conductivity insulation was intended to force the heat necessary for the evaporation process to pass, in large part, through the air–vapor mixture, which is a high-resistance path.

The tube had an i.d. of 6.10 cm, an empty internal length of 20.29 cm, and a wall thickness of 0.2 cm. Thus, the L/d for the empty tube was about 3.3 (virtually the same as that for the isothermal evaporation experiments).

The insulation was enclosed in a cardboard container the external dimensions of which formed a cube 30.5 cm on a side. To facilitate handling the fine aerogel powder, it was first poured into plastic bags and then sealed therein, after which the bags were placed in the cardboard container. A vertical cylindrical cavity, centered in the square planform of the insulation enclosure, was created to house and position the tube. The wall and base of the cavity were made of lightweight cardboard cut from a standard manila folder having a thickness of 0.1 cm.

Instrumentation

Instrumentation was provided to measure six quantities needed for the evaluation of the evaporation rate, mass transfer coefficient, Sherwood number, Rayleigh number, water surface location (relative to the tube opening), and water surface temperature. The measured quantities included temperature, pressure, mass, humidity, water surface location, and time.

Temperature measurements were made at the water surface and in the ambient adjacent to the tube opening. The thermocouples used for these measurements were fabricated from specially calibrated 30-gage, Teflon-coated chromel and constantan wire. Chromel–constantan thermocouples were used because they do not interact with water and because they have the highest thermoelectric sensitivity among all common thermocouple types.

The two thermocouples used for the ambient temperature measurement were respectively positioned 5 and 35 cm above the tube opening and about 2 cm to the side of the opening. Two thermocouples were also used at the water surface. These thermocouples were led in from below, and their junctions were positioned just beneath the surface (about 0.2 cm beneath the surface at the start of a data run) to take account of the surface recession due to evaporation. The positioning was accomplished with the aid of sensitive tweezers. In the non-isothermal evaporation experi-

ments, a third thermocouple was placed at mid-height in the water pool.

All thermocouple outputs were read to within 1 μV by a digital voltmeter. The meter was situated outside the laboratory to enable the readings to be made without disturbing the laboratory ambient.

The pressure was read to within 0.1 mm Hg with a vernier-equipped mercury barometer, and the readings were corrected for temperature according to a chart which accompanied the instrument. The barometer was situated within 2 m of the evaporation apparatus.

Either of two balances was used to measure the mass of the containment tube and its contents before and after an evaporation run. As was discussed earlier, the tube used in the isothermal evaporation experiments was designed to enable the mass measurements to be made with an analytical balance having a 200 g capacity and a resolution of 0.0001 g. The evaporation-related changes of mass measured with this balance were in the 1–2.6 g range.

The weighing chamber of the analytical balance was not high enough to accommodate the height of the polyethylene tube used in the non-isothermal experiments. For that case, the mass measurements were made with a triple-beam balance having a capacity of 2610 g and a resolution of 0.05 g. Since the measured evaporated mass was typically about 5 g, the 0.05 g resolution was acceptable. Both balances were immediately adjacent to the evaporation site, enabling the measurements to be made quickly and in the same ambient as in the experiments proper.

A specially fabricated psychrometric unit was used for the humidity determination. The unit consisted of a 76 cm long, 7.6 cm diameter plexiglass tube equipped at its downstream end with a fan which was operated in the suction mode to draw air through the tube. Dry- and wet-bulb thermometers penetrated the tube wall radially and were positioned with their bulbs on the tube centerline, with the former upstream of the latter and with a separation of 30 thermometer diameters. The thermometers were ASTM certified and could be read to 0.1°F or better.

The tube diameter and the fan of the psychrometric unit were sized to provide near equality of the psychrometric and thermodynamic wet-bulb temperatures. Also, the tube was covered with aluminum foil to eliminate extraneous radiation. In actuality, radiation was not an issue because the psychrometric unit was operated when the laboratory was in complete darkness.

Preliminary experiments had been performed to determine the temperature–time characteristics of the wet-bulb thermometer. With this knowledge, the experimenter could absent himself from the laboratory during the transient period and only enter to take the steady-state temperature readings, and then only with illumination from a small flashlight.

Two methods were used to determine the distance L between the water surface and the top of the containment tube. One method, to be described later in the section on Data Reduction, was a calculation based on mass measurements of the tube with water and the tube without water. The other was a direct measurement using a rigid aluminum scale with precisely ruled subdivisions of 0.5 mm. To facilitate the measurement, the scale was suspended from a tripod equipped with a leveling adjustment. The tripod was positioned so that the scale contacted the water surface in a region well away from the tube wall, thereby avoiding possible meniscus effects at the wall. The two methods yielded L values that were within the accuracy of the direct measurement.

The duration of each data run was measured with an analogue quartz watch able to resolve 0.5 s.

Experimental procedure

Subsequent to the filling of the tube with distilled water, an equilibration period was allowed during which the temperature of the apparatus passed through an initial transient and ultimately became steady with respect to the ambient temperature. For the uninsulated aluminum tube, the end result of the equilibration was virtual equality of the temperatures of the water and the ambient. In the case of the insulated polyethylene tube, the end result was a depression of the water surface temperature below the ambient temperature. Equilibrium was established in about 1 h for the aluminum tube and in about 1–4 h for the insulated polyethylene tube, depending on L/d, with a longer time required at larger L/d.

When sequential evaporation runs were performed, the water level, characterized by L, was varied from run to run by removing a small amount of water. This operation caused virtually no disturbance of the equilibrium condition.

At the beginning of the evaporation run proper, the positions of the thermocouples used to measure the water surface temperature were adjusted with the aid of the tweezers mentioned earlier. Also, at the beginning of the run, measurements were made of the mass of the tube and its contents, water level, humidity in the ambient, temperatures, pressure, and time, and these same quantities were measured at the conclusion of the run. During the run, the temperatures and the pressure were read with instruments situated outside the laboratory. In the longer evaporation runs, i.e. those of 8 h duration, the humidity was measured midway during the run.

The durations of the evaporation runs were selected to yield mass changes of approximately 2 and 5 g, respectively, to be measured by the analytical balance and the beam balance. With the prevailing ambient humidity levels, the run times ranged from 4 to 8 h. The corresponding evaporation-related surface recessions in the aluminum and polyethylene tubes were both about 0.17 cm.

The overriding objective of all aspects of the experimental procedure was to avoid disturbing the laboratory ambient and the equilibrium state of the

apparatus. Thus, the presence of the experimenter in the laboratory was kept to a minimum, and lighting was rarely used and then was confined to a small flashlight. To avoid disturbing the thermal equilibrium state of the tubes, well-insulated ski gloves were used when the tubes had to be touched.

DATA REDUCTION

The methods used to evaluate the evaporative mass transfer coefficient, the Sherwood number, the Rayleigh number, and the water surface location from the experimental data will now be described. The mass transfer coefficient is based on the difference in the densities of the water vapor at the water surface and in the ambient, while the difference in the mixture densities in the ambient and at the surface appears in the Rayleigh number. Therefore, the determination of these densities is a natural starting point of the data reduction.

The partial pressure $p_{wv,\infty}$ of the water vapor in the ambient was calculated from the measured dry- and wet-bulb temperatures and the barometric pressure by using psychrometric equations available in standard textbooks (e.g. pp. 393–397 of ref. [3]). The details of the calculation are presented in ref. [2], where algebraic relations for the participating thermodynamic properties are also set forth. Note that within the accuracy of the instrumentation, the independently measured dry-bulb and ambient temperatures were identical. Then, with the saturation pressure $p_{sat}(T_{db})$ corresponding to the dry-bulb temperature, the ambient relative humidity ϕ_∞ was obtained from

$$\phi_\infty = p_{wv,\infty}/p_{sat}(T_{db}). \tag{1}$$

In turn, ϕ_∞ was used in conjunction with the saturation density at T_{db} to compute the vapor density in the ambient

$$\rho_{wv,\infty} = \phi_\infty \rho_{sat}(T_{db}). \tag{2}$$

The next quantity to be determined is the density ρ_∞ of the air–vapor mixture in the ambient. To this end, the partial pressure of dry air in the ambient is found from $p_{a,\infty} = p - p_{wv,\infty}$, in which p is the barometric pressure. Then, the partial density $\rho_{a,\infty}$ of the dry air is calculated using the perfect gas law and, with this

$$\rho_\infty = \rho_{wv,\infty} + \rho_{a,\infty}. \tag{3}$$

The water vapor and mixture densities at the water surface, $\rho_{wv,s}$ and ρ_s, respectively, will now be determined. For the determination, it will be assumed that the liquid and the adjacent vapor are at a saturation state corresponding to the measured surface temperature T_s. It then follows that

$$\rho_{wv,s} = \rho_{sat}(T_s), \quad p_{wv,s} = p_{sat}(T_s). \tag{4}$$

Furthermore, the partial pressure of dry air adjacent to the surface is

$$p_{a,s} = p - p_{wv,s}$$

and the density $\rho_{a,s}$ is obtained from the perfect gas law. Then

$$\rho_s = \rho_{wv,s} + \rho_{a,s}. \tag{5}$$

If ΔM denotes the mass of water evaporated during a data run and τ is the duration of the run, then the mass transfer coefficient K for evaporation may be defined as

$$K = (\Delta M/A\tau)/(\rho_{wv,s} - \rho_{wv,\infty}) \tag{6}$$

in which A is the surface area $\pi d^2/4$.

The dimensionless counterpart of the mass transfer coefficient is the Sherwood number $Sh = Kd/D$. where D is the mass diffusion coefficient. It is convenient to eliminate D by making use of the definition of the Schmidt number, $Sc = \nu/D$, so that

$$Sh = (Kd/\nu)Sc. \tag{7}$$

The Schmidt number for mixtures of air and water vapor is 0.6.

Since natural convection occurs in the air–vapor space between the liquid surface and the top of the tube, it is of interest to evaluate a characteristic Rayleigh number. In general, both temperature and concentration differences may contribute to the buoyancy which drives the natural convection. Correspondingly, it is appropriate to base the Rayleigh number on a density difference rather than on a temperature difference or a concentration difference, which represent special cases. The Rayleigh number definition used here is

$$Ra = [g(\rho_\infty - \rho_s)d^3/\rho\nu^2]Sc. \tag{8}$$

The density ρ that appears in equation (8) and is embedded in ν $(= \mu/\rho)$ in equations (7) and (8) was evaluated as $(\rho_\infty + \rho_s)/2$. With negligible error, the viscosity was taken as that of dry air at the temperature $(T_\infty + T_s)/2$.

For each evaporation run, the distance L between the water surface and the top of the tube was evaluated from

$$L = (L_1 + L_2)/2 \tag{9}$$

where L_1 and L_2 denote the respective distances at the beginning and the end of the run. This averaging is believed to be altogether acceptable, since $(L_2 - L_1)$ was typically about 0.17 cm, which is small compared with the 3.80 and 6.10 cm respective tube diameters.

The values of L_1 and L_2 were found by direct measurement and, independently, by utilizing the measured mass. With regard to the latter, let M_1 and M_2, respectively, denote the mass of the water in the tube at the beginning and the end of the data run. These quantities were obtained by subtracting the fixed mass of the tube and its auxiliaries from the initial and final measured masses. Then, if H denotes the height of the water in the tube and ρ_{wtr} is the density of the water

$$H_i = [M_i/\rho_{wtr} + V_{tc}]/(\pi d^2/4) \quad (10)$$

in which V_{tc} represents the volume occupied by the thermocouples, and $i = 1, 2$. Furthermore, if L_{max} denotes the top-to-bottom internal depth of the empty tube, then

$$L_i = L_{max} - H_i. \quad (11)$$

The values of L_1 and L_2 determined from equation (11) were used as input to equation (9), which yielded L.

As noted earlier, the two methods of determining L provided results which were in agreement within the accuracy of the direct measurements.

RESULTS AND DISCUSSION

Sherwood numbers

The experiments were performed for three sets of ambient conditions, two of which were for isothermal evaporation and the third of which was for non-isothermal evaporation. These conditions are

$$\text{iso case 1:} \quad T_\infty = 24.6°C, \quad \phi_\infty = 45\% \quad (12a)$$

$$\text{iso case 2:} \quad T_\infty = 23.1°C, \quad \phi_\infty = 17.5\% \quad (12b)$$

$$\text{non-iso:} \quad T_\infty = 24.3°C, \quad \phi_\infty = 14.6\%. \quad (12c)$$

The barometric pressure was typically in the range 735–740 mm Hg. For each of the cases identified in equations (12a)–(12c), data were collected for dimensionless distances between the liquid surface and the top of the tube in the L/d range which extended from as low as 0.2 to as high as 2.85.

For each of the isothermal cases, the Rayleigh number was a constant, equal to 8.2×10^3 and 9.6×10^3 for iso cases 1 and 2, respectively. On the other hand, for the non-isothermal case, the Rayleigh number varied with L/d in response to the variation of the liquid surface temperature with L/d.

The Sherwood number results will now be presented. As noted earlier, the Sherwood number is a dimensionless representation of the evaporation rate. The Sherwood numbers for iso cases 1 and 2 are displayed in Figs. 3 and 4, respectively, while Fig. 5 is for the non-isothermal case. In each figure, Sh is plotted as a function of the dimensionless distance L/d between the liquid surface and the top of the tube.

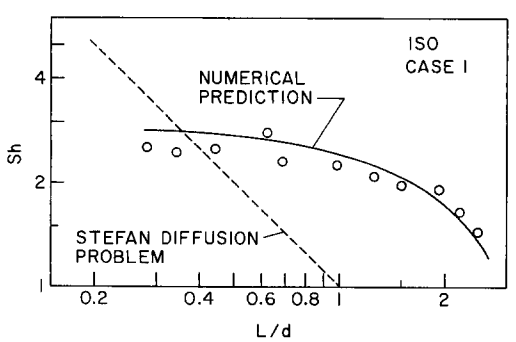

FIG. 3. Sherwood number results for isothermal evaporation (iso case 1).

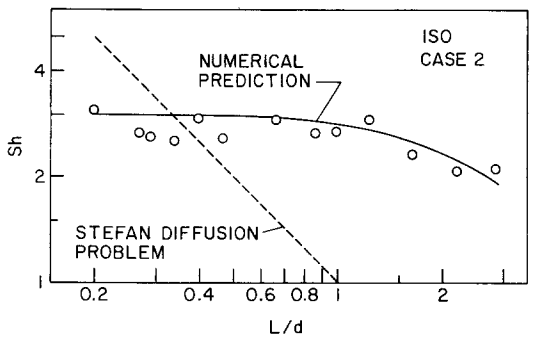

FIG. 4. Sherwood number results for isothermal evaporation (iso case 2).

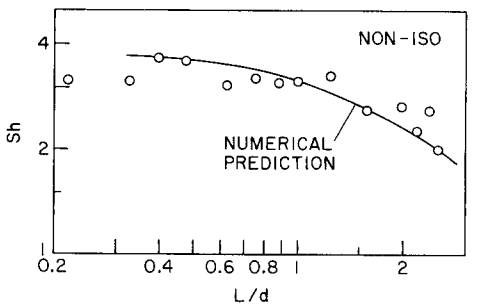

FIG. 5. Sherwood number results for non-isothermal evaporation.

In addition to the experimental data, each figure contains a solid line representing predictions from numerical solutions performed here which were based on models formulated in ref. [1]. In particular, the predictions appearing in Figs. 3 and 4 are based on an isothermal model in which the solution domain encompassed not only the air–vapor space in the tube but also extended into the ambient above the tube (i.e. the ambient-including model). The numerical prediction in Fig. 5 is based on model NI 4 of ref. [1]. That model includes a host of non-isothermal effects but did not include the ambient in the solution domain. Instead, on the basis of exploratory computations documented in ref. [1], the omission of the ambient was compensated by a 5% correction (an increase) of the Sherwood numbers.

Note that the only experiment-related inputs to the computer program were T_∞, ϕ_∞, p_∞, and L/d. In particular, for the non-isothermal case, the liquid surface temperature T_s was not an input but, rather, was determined as part of the solution.

The dashed line appearing in Figs. 3 and 4 represents the solution of the Stefan diffusion problem, for which $Sh = 1/(L/d)$. In the Stefan problem, the only participating transport mechanism is concentration-driven diffusion in the air–vapor space.

An overall inspection of Figs. 3–5 shows that the data and the numerical predictions are mutually highly supportive. In this regard, it is worth reiterating that the models used for the isothermal and non-

isothermal cases are significantly different. Therefore, the comparisons conveyed in the figures provide independent confirmation of both models.

Natural convection in the gas–vapor space between the liquid surface and the top of the tube plays an altogether essential role in both the models, although there are different contributions to the buoyancy for isothermal and non-isothermal conditions. Other features of the non-isothermal model which contribute significantly to the numerically predicted *Sh* values are thermal radiation at the bounding surfaces of the gas–vapor space and natural convection in the liquid pool. The experimental validation of the predicted values of *Sh* serves to confirm the proper modeling and importance of these processes.

The quality of the comparisons serves to recommend the models for subsequent applications. Thus, the major goal of the experimental work—the verification of the models—has been accomplished.

The data and the predictions indicate a common trend with L/d. For small L/d, the Sherwood number (i.e. the evaporation rate) is relatively insensitive to increasing L/d. However, at larger L/d, *Sh* tends to drop off more rapidly with L/d. This trend evidences the increased resistance which corresponds to a longer transfer path between the liquid surface and the ambient.

The moderate scatter of the data reflects deviations from the nominal operating conditions set forth in equation (12). The deviations occurred because the ambient temperature and ambient humidity could not be actively controlled. Rather, as described earlier, the control was passive (e.g. high thermal inertia in the laboratory, thermal insulation and moisture absorption by the cork walls, etc.).

The predictions of the Stefan model (dashed line) appear to be altogether erroneous. The main flaws of this model are the neglect of natural convection and the insufficiency of a one-dimensional treatment, especially when L/d is small.

Liquid surface temperatures

For non-isothermal evaporation, the temperature T_s of the liquid surface varies with the distance between the surface and the top of the tube. The measured and predicted variations of T_s with L/d for the non-isothermal case identified in equation (12c) are presented in Fig. 6. Each data point represents the average of the two surface-contacting thermocouples, while the predicted values correspond to radial averages across the water surface. In addition to the data and the solid line which depicts the predictions, there is a dashed line representing a linear, least-squares fit of the data. For reference purposes, the ambient temperature T_∞ (= 24.3°C) is shown as a horizontal dash-dot line near the top of the figure.

From the figure, it is seen that T_s decreases monotonically with L/d, which is consistent with the expected increase of the thermal resistance between the liquid surface and the ambient. The temperature depression $(T_\infty - T_s)$ at the surface increases from about 2°C to slightly less than 3°C over the investigated range of L/d.

The apparent data scatter in the figure is much exaggerated due to the highly expanded ordinate scale. On the other hand, the least-squares representation of the data is virtually coincident with the numerical prediction. This excellent agreement lends further support to the model on which the predictions are based.

Flow patterns and velocity profiles

Numerically determined fluid flow information corresponding to the operating conditions of the experiments will now be presented. Attention will first be directed to the isothermal evaporation cases, iso 1 and

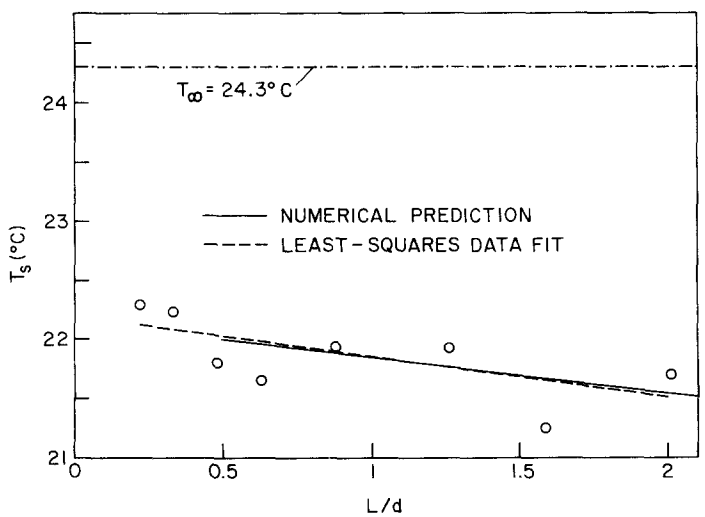

FIG. 6. Liquid surface temperatures for non-isothermal evaporation.

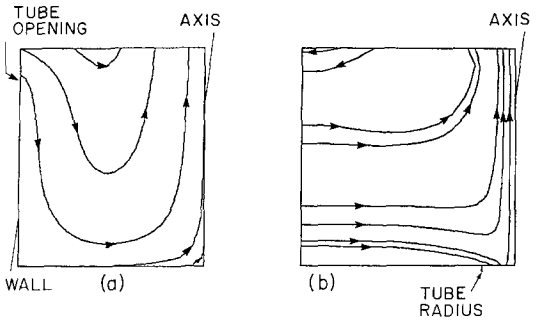

FIG. 7. Patterns of fluid flow for isothermal evaporation (iso case 1) and $L/d = 0.5$: (a) in-tube air–vapor space; (b) ambient.

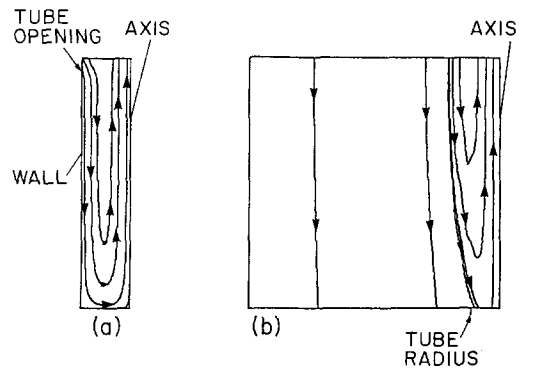

FIG. 8. Patterns of fluid flow for isothermal evaporation (iso case 1) and $L/d = 2.5$: (a) in-tube air–vapor space; (b) ambient.

iso 2, as identified in equations (12a) and (12b). The flow field results for these cases are qualitatively similar, so that only one of them need be considered here—for concreteness, iso 1.

Figures 7 and 8 exhibit flow patterns in the form of streamline maps for iso 1, with Fig. 7 corresponding to $L/d = 0.5$ and Fig. 8 to $L/d = 2.5$. Each figure consists of two diagrams. Diagram (a), on the left, shows representative streamlines in the air–vapor space between the liquid surface and the tube opening and, in addition, in a small portion of the ambient just above the tube opening. The vertical position of the opening is pointed out in the diagram. The right-hand boundary of the diagram is the symmetry axis, the lower boundary is the surface of the liquid, and the left-hand boundary (up to the opening) is the tube wall.

Diagram (b), on the right, shows streamlines in the ambient. The right-hand boundary is the symmetry axis, and the portion of the lower boundary between the axis and the tic mark (designated *tube radius*) coincides with the tube opening. Thus, the two diagrams have difference scales which are readily related by equating the overall horizontal dimension of diagram (a) with the horizontal distance between the tic and the axis on the lower boundary of diagram (b).

The in-tube flow patterns for the two L/d's, as pictured in Figs. 7(a) and 8(a), are qualitatively similar. Fluid from the ambient enters the tube through an annular region adjacent to the wall. The depth to which this fluid penetrates the tube depends on its proximity to the wall—the closer to the wall, the deeper the penetration. The blocking action of the water surface requires that the fluid turn about and, after the turn, it proceeds to exit the tube through a circular core which surrounds the axis. The exiting mass flow exceeds the entering mass flow as a result of the evaporation which occurs at the water surface. Evidence of the evaporation is provided by the streamlines which originate at the surface.

For the $L/d = 0.5$ case, the streamlines are more rounded and the turns are more gradual than for the $L/d = 2.5$ case. For the former, the flow passing through the tube opening possesses a greater transverse component than for the latter.

The flow patterns in the ambient, Figs. 7(b) and 8(b), are markedly different for the two L/d's. For $L/d = 0.5$, there is a significant horizontal flow, a portion of which turns downward into the tube opening. Another portion is turned upward as it is entrained by the jet which is formed by the core-like outflow from the tube. The jet persists as a coherent entity throughout the investigated region of the ambient.

The ambient flow for the $L/d = 2.5$ case has a strongly vertical orientation. The fluid passing from the ambient into the tube is a downflow which pinches in as it enters the opening. Between this downflow and the upflowing jet which emanates from the core of the tube is a zone of recirculation.

In-tube velocity profiles which correspond to the flow patterns of Figs. 7(a) and 8(a) are respectively presented in Figs. 9 and 10 for $L/d = 0.5$ and 2.5 (and for iso 1). In each figure, the axial velocity component u, embedded in the Reynolds-number-like dimensionless group ud/ν, is plotted as a function of the dimensionless radial coordinate r/R. Profiles are shown at four axial stations characterized by both x/L and x/d, where $x = 0$ at the surface of the liquid and $x = L$ at the tube opening. Note that the x/L stations are common to both figures, but the x/d stations are different.

The most noteworthy characteristic of the velocity profiles is their two-lobed nature. Over approximately the inner half of the tube radius, the velocities are positive (upflow), while over the outer half, they are negative (downflow). The integral

$$\int ru\,dr$$

over the cross section is constant for all profiles of a given set, with the constant being proportional to the rate of evaporation at the surface of the liquid.

Each set of velocity profiles reflects a decelerating flow in the direction from the tube opening to the liquid surface, which is in accord with the deployment of the streamlines in Figs. 7(a) and 8(a). The deceleration is slight in the upper half of the $L/d = 2.5$ space (i.e. straight, parallel streamlines), and only in the lower portion of the tube, where there is appreci-

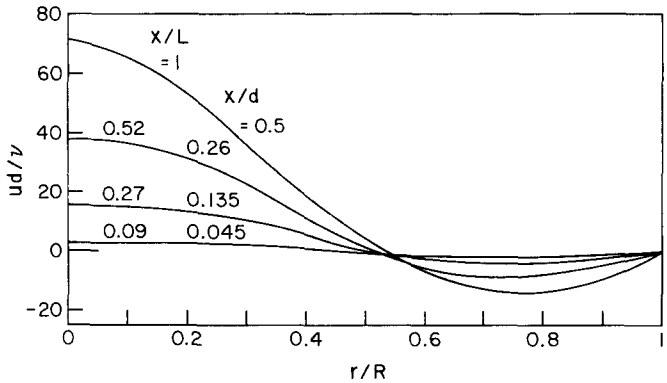

FIG. 9. Velocity profiles in the in-tube air–vapor space for isothermal evaporation (iso case 1) and $L/d = 0.5$.

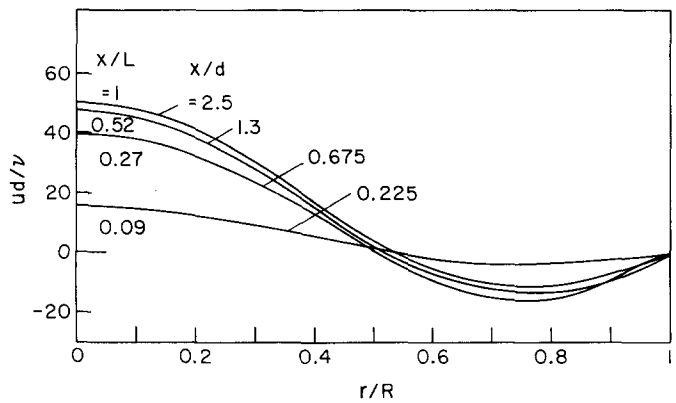

FIG. 10. Velocity profiles in the in-tube air–vapor space for isothermal evaporation (iso case 1) and $L/d = 2.5$.

able turning of the flow, does substantial deceleration occur. On the other hand, for $L/d = 0.5$, deceleration is in evidence at all stations. Note that although higher velocities are attained across the opening for the $L/d = 0.5$ case relative to those for $L/d = 2.5$, the velocities for the former drop off more rapidly with decreasing x than do those for the latter.

Attention is now turned to the case of non-isothermal evaporation for which the operating conditions were specified in equation (12c). Flow patterns and velocity profiles for the non-isothermal case will be presented for $L/d = 0.5$ and 2.5.

As noted earlier, the solution domain for the non-isothermal case did not include the ambient. Therefore, streamline patterns for the ambient are not available. The streamline patterns in the air–vapor space between the liquid surface and the opening of the tube are presented in Fig. 11, with diagrams (a) and (b) for $L/d = 0.5$ and 2.5, respectively. The dimensions of the two diagrams were chosen for presentation compatibility. In reality, the ratio of the horizontal dimensions of diagrams (a) and (b) should be five.

The major novelty conveyed by Fig. 11 is that the direction of the fluid flow is reversed compared with that for isothermal evaporation (see Figs. 7(a) and 8(a) for comparison). Now, the ambient fluid enters the tube through a core-like region which encompasses the axis. The fluid exits the tube through an annular region adjacent to the tube wall.

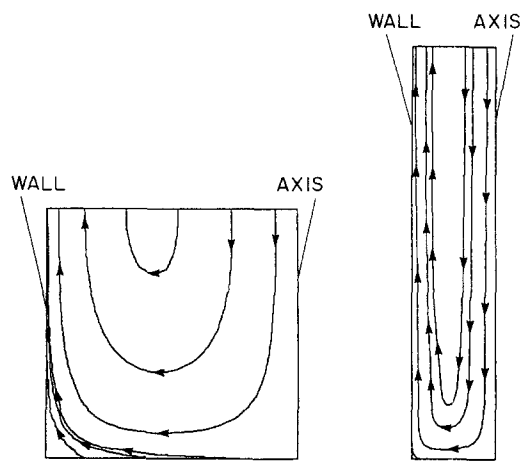

FIG. 11. Patterns of fluid flow in the in-tube air–vapor space for non-isothermal evaporation: (a) $L/d = 0.5$; (b) $L/d = 2.5$.

This reversal, relative to the isothermal case, reflects the rearrangement of the buoyancy field which is brought about by the participation of the temperature. It is believed that the vertical upward tem-

perature increase at the tube wall is a major factor in establishing the direction of the fluid flow. The upward acceleration at the wall demands an upflow there, and the remainder of the flow field must arrange itself in accordance with continuity.

One consequence of the reversed pattern is that the air–vapor flow sweeps radially outward across the surface of the liquid. This flow direction was verified experimentally by placing chalk dust at the center of the liquid surface at the beginning of a non-isothermal evaporation run. At the end of the run, it was observed that the dust had migrated to the tube wall.

Aside from the reversed flow direction, the streamline patterns of Fig. 11 are qualitatively similar to those of Figs. 7(a) and 8(a). However, in Fig. 11, the streamlines are perpendicular to the tube opening, while those of Figs. 7(a) and 8(a) deviate somewhat from the perpendicular. The perpendicularity was, in fact, a feature of the model used to disconnect the tube from the ambient in the non-isothermal case.

Velocity profiles that are the counterparts of the flow patterns of Fig. 11 are presented in Figs. 12 and 13, respectively for $L/d = 0.5$ and 2.5. The profiles are again of the two-lobe type, but now with negative velocities (downflow) in the inner lobe and positive velocities (upflow) in the outer lobe.

As before, the largest velocity magnitudes occur at the tube opening, with lesser magnitudes encountered at axial stations that are situated progressively farther from the opening (i.e. decreasing x). For $L/d = 0.5$, the velocity decrease is appreciable over the entire range of axial stations considered, reflecting the deceleration associated with the early turning of the flow. On the other hand, for $L/d = 2.5$, the decrease of the velocity magnitudes is moderate for the considered stations. This is in accord with the fact that the turning is primarily confined to axial stations adjacent to the surface of the liquid.

CONCLUDING REMARKS

The experiments reported here were undertaken to provide a critical test of analytical/numerical models formulated to predict evaporation of a liquid which partially fills an open-topped vertical tube. The models, described in ref. [1], encompassed both isothermal and non-isothermal evaporation. Correspondingly, separate apparatuses were employed to achieve these two modes of evaporation. The experiments were performed for the evaporation of water into air which contained water vapor. In addition to the experimental work, the models were numeri-

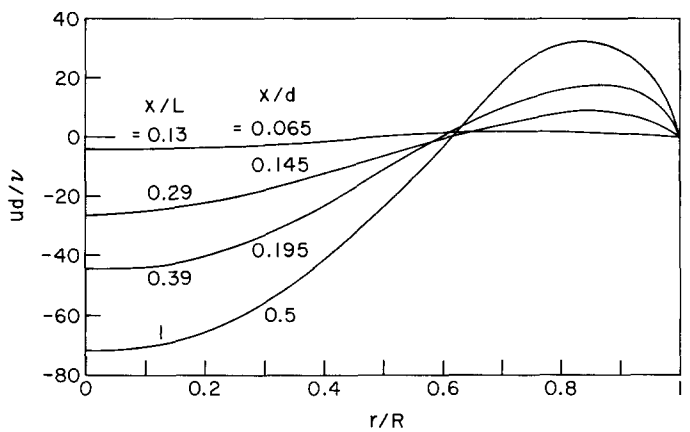

FIG. 12. Velocity profiles in the in-tube air–vapor space for non-isothermal evaporation and $L/d = 0.5$.

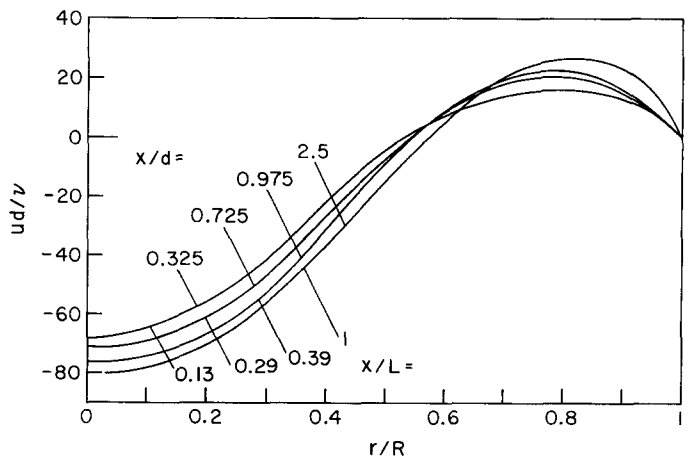

FIG. 13. Velocity profiles in the in-tube air–vapor space for non-isothermal evaporation and $L/d = 2.5$.

cally implemented for the ambient conditions of the experiments.

A comparison of the experimentally determined and numerically predicted Sherwood numbers revealed excellent agreement, thereby validating the models. The validation of the models settles a number of key issues. For isothermal evaporation, it is now established that diffusion-driven transport alone, as in the Stefan diffusion problem, is insufficient, and that natural convection in the gas–vapor space must be taken into account. For non-isothermal evaporation, in addition to natural convection in the gas–vapor space, account must be taken of radiation at the bounding surfaces of the gas–vapor space and of natural convection in the liquid pool.

REFERENCES

1. G. A. Nunez and E. M. Sparrow, Models and solutions for isothermal and non-isothermal evaporation from a partially filled tube, *Int. J. Heat Mass Transfer* **31**, 461 477 (1988).
2. G. A. Nunez-Testa, Evaporation in the presence of isothermal and non-isothermal natural convection, Ph.D. thesis, Department of Mechanical Engineering, University of Minnesota, Minneapolis, Minnesota (1986).
3. W. C. Reynolds and H. C. Perkins, *Engineering Thermodynamics*, 2nd Edn. McGraw-Hill, New York (1977).

EXPERIENCES SUR L'EVAPORATION ISOTHERME OU NON A PARTIR DE TUBES VERTICAUX PARTIELLEMENT REMPLIS ET OUVERTS AU SOMMET

Résumé—Des expériences sont conduites pour fournir un test critique à des modèles analytiques/numériques qui prédisent l'évaporation pour des tubes verticaux ouverts au sommet et partiellement emplis de liquide. Des appareils séparés permettent l'évaporation, dans des conditions soit isothermes soit non isothermes, d'eau dans l'air constant de la vapeur d'eau. Un accord excellent est trouvé entre les nombres de Sherwood expérimentaux et calculés. Cela ajouté à d'autres comparaisons valide les modèles. Pour l'évaporation isotherme, la validation établit que l'on doit prendre en compte la convection naturelle dans le mélange gaz–vapeur au dessus de la surface du liquide et que la diffusion pure est une description insuffisante du mécanisme de transfert. Pour l'évaporation non isotherme, en plus de la convection naturelle dans l'espace gaz–vapeur, il est nécessaire de prendre en compte le rayonnement thermique des surfaces qui limitent l'espace et la convection naturelle dans le bain liquide.

VERSUCHE ZUR ISOTHERMEN UND NICHT-ISOTHERMEN VERDUNSTUNG AUS TEILWEISE GEFÜLLTEN, NACH OBEN OFFENEN, SENKRECHTEN ROHREN

Zusammenfassung—Um eine kritische Überprüfung eines analytisch-numerischen Modells zur Berechnung der Verdunstung aus mit Flüssigkeit gefüllten, nach oben offenen, senkrechten Rohren vorzunehmen, wurden Versuche durchgeführt. Unterschiedliche Apparaturen wurden benutzt, um die Verdunstung sowohl unter isothermen als auch unter nicht-isothermen Bedingungen ablaufen zu lassen. Die experimentelle Arbeit wurde durch die numerische Implementierung des Modells, für das die Umgebungsbedingungen der Versuche als Eingabedaten benutzt wurden, ergänzt. Zwischen den experimentell bestimmten und den numerisch ermittelten Sherwood-Zahlen ergab sich eine sehr gute Übereinstimmung. Diese Erkenntnis bestätigte zusammen mit anderen Vergleichen das Modell. Für isotherme Verdunstung wurde durch die Validierung festgestellt, daß die natürliche Konvektion im Gas/Dampf-Raum über der Flüssigkeitsoberfläche berücksichtigt werden muß, und daß reine Diffusion die Transportprozesse unzureichend beschreibt. Für nicht-isotherme Verdunstung wurde die Notwendigkeit festgestellt, zusätzlich zur natürlichen Konvektion im Gas/Dampf-Raum die Strahlung an den Begrenzungsflächen des Raumes und die natürliche Konvektion in der Flüssigkeit zu berücksichtigen.

ЭКСПЕРИМЕНТЫ ПО ИЗОТЕРМИЧЕСКОМУ И НЕИЗОТЕРМИЧЕСКОМУ ИСПАРЕНИЮ ИЗ ЧАСТИЧНО ЗАПОЛНЕННЫХ ВЕРТИКАЛЬНЫХ ТРУБ С ОТКРЫТЫМ ВЕРХНИМ ТОРЦОМ

Аннотация—Проведены эксперименты по проверке аналитических и численных моделей расчета испарения из вертикальных частично заполненных жидкостью труб с открытым верхним торцом. Изотермические и неизотермические условия испарения получены с помощью различных установок. Эксперименты проводились с водой, испаряющейся в воздух, содержащий пары воды. Экспериментальные исследования дополнялись применением численного моделирования, в котором условия окружающей среды принимались в качестве входных данных. Получено очень хорошее соответствие между значениями числа Шервуда, полученными экспериментально и численно. Это совпадение наряду с другими доводами обосновывает пригодность модели. Для случая изотермического испарения показана необходимость учета естественной конвекции в газо-паровом пространстве над поверхностью жидкости и недостаточность чистой диффузии для описания процесса переноса. Для случая неизотермического испарения найдено, что кроме естественной конвекции в газо-паровом пространстве необходимо принимать во внимание тепловое излучение на граничных поверхностях и естественную конвекцию в объеме жидкости.